Structural and Biochemical Analysis of *Escherichia coli* ObgE, a Central Regulator of Bacterial Persistence

Sotirios Gkekas‡§, Ranjan Kumar Singh‡§, Alexander V. Shkumatov‡§, Joris Messens‡§, Maarten Fauvart¶, Natalie Verstraeten¶, Jan Michiels¶ and Wim Versées‡§**

From ‡Structural Biology Brussels, Vrije Universiteit Brussel, 1050 Brussels, Belgium, the §VIB-VUB Center for Structural Biology, 1050 Brussels, Belgium, the ¶Centre of Microbial and Plant Genetics, KU Leuven - University of Leuven, 3001 Leuven, Belgium and the **Department of Life Science Technologies, Smart Systems and Emerging Technologies Unit, imec, 3001 Leuven, Belgium

Running title: *Structural and Biochemical Analysis of ObgE*

To whom correspondence should be addressed: Prof. Dr. ir. Wim Versées, Structural Biology Brussels, Vrije Universiteit Brussel, Pleinlaan 2, 1050 Brussels, Belgium. Telephone: +32 2 629 18 49; FAX: +32 2 629 19 63; E-mail: wim.versees@vib-vub.be

ABSTRACT

The Obg protein family belongs to the TRAFAC (translation factor) class of P-loop GTPases and is conserved from bacteria to eukaryotes. Essential roles in many different cellular processes have been suggested for the Obg protein from *Escherichia coli* (ObgE), and we recently showed that it is a central regulator of bacterial persistence. Here, we report the first crystal structure of ObgE at 1.85 Å resolution in the GDP-bound state, showing the characteristic N-terminal domain and a central G domain that are common to all Obg proteins. ObgE also contains an intrinsically disordered C-terminal domain, and we show here that this domain specifically contributed to GTP binding, while it did not influence GDP binding or GTP hydrolysis. Biophysical analysis, using small angle X-ray scattering and multi-angle light scattering experiments, revealed that ObgE is a monomer in solution, regardless of the bound nucleotide. In contrast to recent suggestions, our biochemical analyses further indicate that ObgE is neither activated by K^+ ions nor by homodimerization. However, the ObgE GTPase activity was stimulated upon binding to the ribosome, confirming the ribosome-dependent GTPase activity of the Obg family. Combined, our data represent an important step toward further unraveling the detailed molecular mechanism of ObgE, which might pave the way to further studies into how this GTPase regulates bacterial physiology, including persistence.

Guanine nucleotide binding proteins (GNBPs, G proteins or GTPases) are ubiquitously found in all living organisms where they are known to play essential roles in a myriad of cellular processes, including protein synthesis and translocation, membrane trafficking, development, signal transduction and cell cycle control (1–3). G proteins share a common structural module, the G domain that acts as a molecular switch by cycling between a GDP-bound "off" state and a GTP-bound "on" state. Both states mainly differ in the conformation of two regions (Switch I and II), allowing reversible interaction and activation of downstream effector proteins (4, 5).

In the intensively studied small GTPases of the Ras family, nucleotide exchange is very slow and exchange of GDP for GTP is stimulated by guanine nucleotide exchange factors (GEFs) (6, 7). Moreover, the intrinsically slow GTP hydrolysis is accelerated through the interaction with GTPase activating proteins (GAPs) (6, 8). The latter proteins stabilize and / or complement the active site of the GTPase by providing one or two catalytic residues in trans that counter negative charge development at the phosphate groups of GTP or orient the nucleophilic water molecule during hydrolysis (4, 6, 8). More recently a number of other activation mechanisms of G proteins have been described. One class of G proteins is activated through homo- or heterodimerization of their G-domains, hence reciprocally activating each other (9–11). This

class of G proteins is known as the G proteins activated by nucleotide dependent dimerization (GAD) class (12). Another expanding family of G proteins recruits specific cations (such as K^+) to stabilize the GTPase transition state (13–16). Some G proteins use a combination of the two above strategies, as is the case for MnmE, a G protein involved in tRNA modification (17).

The Obg family belongs to the TRAFAC (for translation factor) class of P-loop GTPases and consists of high molecular weight proteins like Obg/CgtA, YchF/YyaF, Drg/Rbg, Nog1 and Ygr210 (3). Among them, Obg is a highly versatile GTPase that is conserved in bacteria, as well as in many eukaryotes (18). Obg displays a three-domain arrangement with an N-terminal glycine rich domain typical for Obg (Obg domain), a central G domain and a C-terminal domain that is highly variable in length and sequence among Obg proteins from different species (19, 20). Obg homologs are widely present in eukaryotic organelles, including chloroplasts and mitochondria (21–23). However, in contrast to bacterial Obg, the rice homolog OsYchF and the human homolog hOLA1 (<u>h</u>uman <u>O</u>bg-<u>l</u>ike <u>A</u>TPase 1) were found to bind and hydrolyze ATP more efficiently than GTP (24, 25). Obg displays a very low GTP hydrolysis rate in combination with a high guanine nucleotide exchange rate, seemingly abrogating the need for GEFs (3, 26). No "classical" Obg-specific GAP proteins have so far been described, although the 50S ribosomal subunit has recently been found to increase the GTPase activity of Obg (27). Furthermore, it has been proposed, based on sequence analysis, that Obg might belong to the class of G proteins that is specifically activated by K^+ ions (15).

Obg was originally discovered in *Bacillus subtilis,* where it was shown to have a critical role in sporulation (28). Moreover, Obg expression was found to be essential for viability in nearly all bacterial species (3, 26), and various functions including ribosome assembly and maturation, cell cycle control, DNA replication, stress response, sporulation and morphological development have been proposed (29–34). The role of Obg in the cellular response to environmental stress is particularly interesting (27, 33, 35–37). Recently, we showed that, in *Escherichia coli* as well as in *Pseudomonas aeruginosa*, Obg plays a central role in the regulation of bacterial persistence in response to nutrient starvation (38). Although the underlying mechanisms need further elucidation, Obg-mediated persistence depends on the presence of the alarmone (p)ppGpp and proceeds through induction of the expression of the HokB toxin.

Here, we report the first crystal structure of Obg from *E. coli* (ObgE) bound to a GDP molecule at 1.85 Å resolution. SAXS and MALS experiments reveal that ObgE behaves as a monomer in solution. A detailed biochemical analysis confirms that ObgE has a modest affinity for nucleotides and ppGpp and fast guanine nucleotide dissociation rates, combined with a low GTP hydrolysis rate. Interestingly, we show that the C-terminal intrinsically disordered domain plays a role in GTP binding, while deletion of this region has a negligible effect on GDP and ppGpp binding and GTP turnover. Finally, kinetic experiments show that ObgE is neither activated by K^+ ions, nor by homodimerization, in contrast to what was previously suggested (15, 20). However, we do observe a weak but significant stimulation of the ObgE GTPase activity by the (70S) ribosome. Together, these data provide new insights into the structure and function of ObgE and will be instrumental to drive further studies aiming to unravel the role of Obg in bacterial persistence.

RESULTS AND DISCUSSION

Overall structure of GDP-bound ObgE - *E. coli* Obg (ObgE) is a 390 amino acid protein that is predicted to consist of a conserved N-terminal glycine-rich Obg domain (amino acids 1-157) followed by a central Ras-like G domain (amino acids 158-340), in analogy to the previously reported crystal structures of Obg from *B. subtilis* and *Thermus thermophilus* (19, 20). In most Obg proteins, these two domains are followed by a third domain, which is much less conserved. Unlike the proteins from *B. subtilis* and *T. thermophilus*, in ObgE this domain consists of a stretch of amino acids (341-390) that are composed for 60% of charged amino acids and are predicted to be intrinsically disordered (Fig. 1a) (39, 40). So far, the function of the latter domain remains largely enigmatic.

In order to allow a straightforward interpretation of biochemical and biological data on *E. coli* ObgE we set out to solve its crystal structure. However, all attempts to crystallize the full length protein (ObgE_FL) failed so far, probably due to the presence of the intrinsically disordered C-terminus. Therefore, we decided to generate a C-terminal deletion construct (ObgE_340) lacking the last 50 amino acids, by replacing the codon for amino acid E341 by a stop

codon. This protein was crystallized successfully in the presence of Mg^{2+} ions and GDP in space group $C222_1$ with one molecule in the asymmetric unit, allowing to solve its crystal structure at a resolution of 1.85 Å by molecular replacement. We were able to confidently build 334 of the 340 amino acids in the electron density map. Residues 133-136, corresponding to a loop region in the Obg domain and the C-terminal residues 339-340, were not built due to weak electron density. The crystal structure clearly shows density for a molecule of GDP and a Mg^{2+} ion in the G domain. The final model has a crystallographic R factor of 0.198 and a free R factor of 0.239 (Table 1).

The crystal structure of ObgE_340 shows the typical arrangement of an N-terminal "Obg domain" followed by a Ras-like G domain (Fig. 1b). Similar to *B. subtilis* and *T. thermphilus* Obg, two regions can be discerned in the Obg domain: a region with six left-handed type II helices connected on one side by long loops, and an eight-stranded β-barrel containing an α-helix between the second and the third strand (19, 20). This β-barrel makes extensive contacts with the G domain. The largest differences in this domain comparing ObgE to the proteins from *B. subtilis* and *T. thermophilus* are present in two of the three long loops connecting each pair of type II helices.

The G domain of ObgE displays a Ras-like fold, consisting of a six-stranded β-sheet and five α-helices. Superposition of the G domain of ObgE on the corresponding domains of *T. thermophilus* and *B. subtilis* Obg (Fig. S1) shows that the biggest differences in conformation are localized in the Switch I and II regions. In the GDP-bound structure of ObgE, both Switch loops could be fully traced, although they are in an "open" conformation where they do not interact with the nucleotide. However, interactions are made between both Switch regions and the N-terminal Obg domain. The Switch II region is folded in two helices, classically termed α_1' and α_2'. The conformation of the Switch loops of GDP-bound ObgE most closely resembles the conformation of these loops in the nucleotide-free protomer of the *B. subtilis* Obg crystal structure, while especially Switch II adopted a different conformation in the *T. thermophilus* crystal structure, mainly due to partial unwinding of helix α_1'. In the ppGpp-bound protomer of *B. subtilis* Obg the Switch regions could not be fully traced (19, 20).

Crystal structures of Obg available in the PDB are either bound to ppGpp (*B. subtilis* Obg) or show Obg in the apo state (*B. subtilis* and *T.*

thermophilus Obg). Here we report the first high resolution structure of ObgE bound to GDP. GDP is anchored tightly to the G domain of ObgE_340 via interactions with residues from the P-loop and the G4 and G5 motif (Fig. 1c, d). The α- and β-phosphates are bound by the P-loop, with the α-phosphate interacting with T174 (side chain and main chain) and the β-phosphate with N169 (main chain), G171 (main chain), K172 (side chain and main chain) and S173 (side chain and main chain). Specificity for the guanine nucleotide is provided by the G4 motif via interactions with N283 (with the N7 of guanine) and D286 (interactions with the N1 and N6 of guanine), and by the G5 motif via interactions of the guanine O6 carbonyl with S314, A315 and A316 (main chain).

ObgE is a monomer in solution - In the crystal structure, the G domain of ObgE_340 interacts with the G domain of the crystal symmetry neighbor. This interface buries a surface area of 836 Å^2 and is mainly formed by interactions between residues of the P-loop and the first α-helix (6 residues), Switch I (10 residues) and Switch II (7 residues), where the Switch I of one protomer interacts with Switch II of the adjacent protomer and *vice versa* (Fig. 2a and S2). This orientation places one arginine residue (R177) of the first α-helix as well as one lysine residue (K183) of the Switch I into the GDP/GTP binding pocket of the neighboring protomer (Fig. 2b). The orientation of the amino group of K183 is reminiscent of the position of the guanido group of the catalytic "arginine finger" (R789) in the Ras-RasGAP complex (Fig. 2c, see further) (41). This observation raises the intriguing question whether ObgE could form a dimer in solution, where two adjacent G domains could reciprocally enhance each other's GTPase activity. Interestingly, a functional dimerization was previously also suggested for the Obg protein from *T. thermophilus*, where the C-terminal domain of one protomer was found to interact with the G domain of the adjacent protomer (20).

To determine the oligomeric state of ObgE_340 and ObgE_FL in solution, first small angle X-ray scattering experiments coupled to size exclusion chromatography (SEC-SAXS) were performed using the proteins in a nucleotide-free form (Fig. 3). The SEC-SAXS profile of ObgE_340 shows a symmetric peak with a constant radius of gyration (R_g) across the elution peak (Fig. S3a). An average R_g (from Guinier analysis) and maximal intramolecular distance (D_{max}) of 30.9 Å and 108 Å, respectively, is

3

obtained which is very close to the R_g and D_{max} values calculated from the crystal structure of an ObgE_340 monomer (R_g =29 Å, D_{max}=110 Å). Furthermore, the molecular mass obtained from the Porod Volume is 41 kDa, while the molecular mass derived from the Porod invariant (Q_R) is 36 kDa (42) (Table S1). These molecular mass estimations match very well with the theoretical monomer molecular mass of 39.1 kDa calculated from the protein sequence, indicating that ObgE_340 mainly adopts a monomeric form in solution. Subsequently, SAXS was also used to determine the molecular mass of ObgE_FL (Fig. 3 and Fig. S4a). The SAXS data of ObgE_FL in a nucleotide-free state yield R_g (from Guinier analysis) and D_{max} values of 37.0 Å and 160 Å, respectively, while the molecular mass estimation from the Porod Volume gives a value of 60 kDa (Table S1). The latter value is higher than the expected value for an ObgE_FL monomer (45.4 kDa). The overestimation of the molecular mass using the Porod Volume and the large values of R_g and D_{max} are however in agreement with the presence of an intrinsically disordered C-terminal domain which occupies a large volume in solution (see further). Correspondingly, calculation of the molecular mass using the Porod invariant (Q_R) gives a molecular mass of 44.8 kDa, which is much closer to the theoretical molecular mass of an ObgE_FL monomer. Together these data show that ObgE in its nucleotide-free state behaves as a monomer in solution.

To further test whether dimerization could potentially occur upon nucleotide binding, we also collected SAXS data of ObgE_340 and ObgE_FL in the presence of an excess of GDP or of the nucleotide triphosphate analogue GppNHp (Fig. S3-S6). Calculation of the molecular mass using the Porod invariant (Q_R) yields values of 47.3 kDa and 34 kDa for ObgE_FL and ObgE_340 in the presence of GDP and 45.1 kDa and 37.7 kDa for ObgE_FL and ObgE_340 in the presence of GppNHp, again very close to the expected monomer molecular masses of 45.4 kDa and 39.1 kDa (Table S1). Finally, the molecular mass of ObgE_FL (apo), ObgE_FL in the presence of GppNHp, and ObgE_FL in the presence of the transition state analogue GDP-AlF$_x$ was further validated using SEC-MALS. SEC-MALS gave a monodisperse peak with apparent molecular mass in the range of 49-51 kDa (Fig. S7), again close to the value expected for a monomer (45.4 kDa). Together, we can conclude from these experiments that ObgE behaves mainly as a monomer in solution,

regardless of concentration and nucleotide state. This is a strong indication that the dimeric form observed in the crystal structure, generated from crystallographic symmetry operations, is a crystallographic artifact. However, at this point we cannot completely exclude that very transient dimer interactions do occur (see further).

Interdomain orientation and influence of nucleotides on the conformation of ObgE - While the individual Obg and G domains of the Obg crystal structures from *E. coli* (this study), *B. subtilis* (19) and *T. thermophilus* (20) superimpose very well (see above), the relative orientation of these domains in the crystal structures differs. Indeed, it had been noted before that upon superimposing the G domains of *B. subtilis* (nucleotide-free or ppGpp bound) and *T. thermophilus* (nucleotide-free) Obg, the respective Obg domains are rotated by about 180° around the G domain axis (20). Moreover, in a low resolution (5.5 Å) EM structure of *E. coli* Obg, bound to the 50S ribosomal subunit, an orientation of the Obg domain intermediate to that observed in *B. subtilis* Obg and *T. thermophilus* Obg was observed (27). A recent molecular dynamics study suggested that the relative orientation of the Obg domain vis-à-vis the G domain changes depending on the nucleotide state of the protein, with the largest difference occurring in the GDP-bound state compared to the apo and GTP-bound states (43). However, in the current high resolution structure of ObgE_340 bound to GDP, the orientation of the Obg domain with respect to the G domain is very similar to the *B. subtilis* Obg structure, either in the apo state or bound to ppGpp (Fig. S1).

To further investigate the influence of nucleotides on the conformation of *E. coli* ObgE_340 and ObgE_FL in solution we again turned to SAXS. To test whether our crystal structure corresponds to a main conformation in solution, we first compared the theoretical scatter curve of the ObgE_340 crystal structure, after flexible modeling of the N-terminal purification tag, with the experimental scatter curve (Fig. S8). Since both curves overlay very well, we can conclude that the crystal structure indeed represents a relevant conformation in solution. Next, we compared the scattering curves of both ObgE_340 and ObgE_FL bound to GDP or GppNHp to the corresponding curve of the nucleotide-free protein (Fig. S5 and S6). This superposition does not reveal any significant nucleotide-dependent changes in the scattering curves, although small differences are observable

when comparing the pair-distance distribution functions and dimensionless Kratky plots of ObgE_FL in different nucleotide states (Fig. S5 and S6). These data seem to indicate that no large-scale nucleotide-induced conformational changes are taking place in *E. coli* ObgE. However, alternatively, it remains possible that such changes only take place in the presence of certain partner proteins, such as the ribosome (27), or that the suggested rotation of the Obg domain vis-à-vis the G-domain does not lead to an observable difference in the low-resolution spherically averaged SAXS profiles. High-resolution crystal structures of ObgE in different nucleotide-bound states could shed further light on this issue.

Conformation and role of the C-terminal domain - The last 50 C-terminal amino acids of ObgE_FL are mainly composed of charged amino acids (about 60%) and are predicted to be intrinsically disordered (39, 40). The flexible disordered nature of this peptide region is also in agreement with our SAXS data for ObgE_FL (see above), which show that (i) the calculated Porod Volume is at least 15% higher than would be expected for a compact monomeric protein, and (ii) the normalized Kratky plot has a broader peak and converges at higher angle than the corresponding plot for ObgE_340 (Fig. 3c). Correspondingly, we did not succeed in crystallizing the full length ObgE protein. Consequently, so far no information regarding the structure and function of this C-terminal domain is available. In order to get an idea of the conformational space adopted by the C-terminal domain in solution, we used the experimental SAXS data of the full length ObgE, in combination with our partial crystal structure and the amino acid sequence, to perform ensemble modeling. The conformation of the last 50 residues was probed using all-atom modeling, followed by model validation using the Molprobity score and further refinement using iterative normal mode analysis (NMA). Model selection based on the experimental SAXS data indicated that the latter could be accounted for by an ensemble of 5 models as depicted in Fig. 4. However, we would like to stress, that the presented ensemble only gives a representative subset of possible orientation of the C-terminal domain in solution that is consistent with the experimental scattering data.

In order to investigate the function of this intrinsically disordered C-terminal domain we determined its contribution to nucleotide binding and hydrolysis by comparing the full-length protein with the C-terminal deletion construct ObgE_340. First, we determined its contribution to nucleotide binding affinity and kinetics using stopped-flow fluorescence experiments (using mant-labelled nucleotides). In agreement with previous reports (35), we find that ObgE_FL displays a relatively low affinity for GDP ($K_D = 0.18 \pm 0.01\,\mu M$) and GTP ($K_D = 0.37 \pm 0.16\,\mu M$) due to fast nucleotide binding and dissociation (see Fig. 5 for all data). Deletion of the C-terminal domain (ObgE_340) leads to a small decrease in affinity for GDP ($K_D = 0.46 \pm 0.02\,\mu M$), while the affinity for GTP is decreased more than 10-fold ($K_D = 4.21 \pm 0.46\,\mu M$). This decrease in affinity is nearly entirely due to an increased GTP dissociation rate (k_{off}(GTP, ObgE_FL) $= 0.44 \pm 0.19$; k_{off}(GTP, ObgE_340) $= 3.67 \pm 0.31$; Fig. 5).

Subsequently, considering that ppGpp is required for ObgE-mediated persistence (38), we also determined the affinity of ObgE_FL and ObgE_340 for ppGpp using ITC experiments (Fig. 6 and Fig. S9). ObgE_FL binds ppGpp with a $K_D = 0.66 \pm 0.03\,\mu M$. Deletion of the C-terminus leads to a very small decrease in affinity for ppGpp ($K_D = 0.78 \pm 0.07\,\mu M$), in agreement with the observed small effect of the C-terminal domain on GDP binding.

Finally, we also assessed the influence of the C-terminal domain on GTP turnover. To this end we measured Michaelis-Menten kinetics. ObgE_FL has a $k_{cat} = 0.064 \pm 0.001\,min^{-1}$ and a $K_M = 10.40 \pm 0.70\,\mu M$, compared to a $k_{cat} = 0.046 \pm 0.001\,min^{-1}$ and a $K_M = 11.07 \pm 0.92\,\mu M$ for ObgE_340 (Table 2 and Fig. S10). This indicates that while the C-terminus is involved in GTP binding, it is not substantially involved in GTP turnover.

In conclusion, we show here that the intrinsically disordered C-terminal domain of *E. coli* ObgE specifically contributes to GTP binding with very little effect on GDP or ppGpp binding. Such a discriminatory effect of the C-terminal domain on GTP versus GDP binding seems to indicate that this domain transiently folds back on the G domain in the GTP-bound state. Such a conformational change of the C-terminal domain is however not reflected in large changes in our SAXS profiles (see above), and further research is required to reveal the underlying mechanisms.

Testing potential GTPase-activating mechanisms of ObgE - ObgE, and Obg proteins in general, show a very low intrinsic GTPase activity (k_{cat} (ObgE) $= 0.064\,min^{-1}$, Table 2). Classically, the rate of GTP hydrolysis of small Ras-like GTPases is enhanced by dedicated GAPs (6, 8).

However, so far no such GAPs for Obg have been reported, although it was recently described that the GTPase activity of Obg is increased upon binding to the ribosome (27, 43). Moreover, recently a number of alternative mechanisms to increase the GTPase activity of G proteins have been reported, including binding of specific ions and reciprocal complementation of active sites by homodimerisation (9–16).

With respect to a potential mechanism of GTPase activation though homodimerization, we were particularly triggered by the observation of a potential homodimer in the ObgE_340 crystal structure, formed through crystal symmetry (see above). This dimeric organization would place both an arginine (R177) and a lysine residue (K183) coming from respectively the first α-helix and the Switch I region of one subunit into the GTP-binding pocket of an adjacent subunit (Fig. 2b). Despite our observation that ObgE_340 is mainly monomeric in solution (see above), it can *a priori* not be excluded that a transient dimeric complex could be formed, where K183 and R177 would function as a catalytic lysine or arginine "finger" by electrostatically stabilizing the GTPase transition state in the adjacent subunit. Such a catalytic role of K183 and/or R177 would be reminiscent of the catalytic "arginine finger" (R789) used by the RasGAP protein for activation of the Ras GTPase activity (41). Even more intriguingly in this respect we find that superposition of the G domain of ObgE_340 onto Ras in the Ras-RasGAP complex (41) places the amino group of K183 from the adjacent ObgE subunit nearly perfectly on the guanidino group of the catalytic arginine finger of the RasGAP protein (Fig. 2c). To test whether K183 or R177 contribute to GTP hydrolysis, we mutated both residues to alanine in ObgE_FL, and compared the steady state kinetic parameters to the wild type protein (Table 2 and Fig. S10). These data show that the K183A mutation lowers k_{cat} by a factor of 3, while the K_M value is nearly unaffected (k_{cat} = 0.020 ± 0.000 min^{-1}; K_M = 10.27±0.75 µM). On the other hand, the R177A mutant has unaffected k_{cat} and K_M values (k_{cat} = 0.060 ± 0.002 min^{-1}; K_M = 6.63 ± 0.69 µM). We thus conclude that, although the K183A mutation has a somewhat lowered k_{cat} value, the observed effects are too small to account for a genuine catalytic finger.

While many small GTPases use an arginine finger from a GAP protein to stabilize the transition state of GTP hydrolysis, other G proteins including MnmE, YqeH, FeoB, RbgA and EngA bind a K$^+$ ion in the active site to neutralize the negative charge of the transition state (13, 14, 44–46). Based on sequence analysis and the presence of an asparagine residue in the so-called K-loop of the Switch I region, Obg proteins were recently proposed to be potential members of these so-called potassium-selective cation-dependent GTPases (15). However, so far this hypothesis has not been experimentally validated. In order to investigate the effect of K$^+$ ions on the kinetic constants of ObgE, the Michaelis-Menten kinetic parameters of ObgE_FL were determined in the presence of 150 mM KCl and compared to those in the presence of 150 mM NaCl (Table 2 and Fig. S10). A small (less than 2-fold) decrease in k_{cat} is observed in presence of KCl compared to NaCl. Therefore, we can rule out a mechanism whereby K$^+$ acts as a GTPase activating factor.

Since we did not find any activation via dimerization or K$^+$ binding, we also reinvestigated the reported effect of the ribosome. Indeed, it was recently shown that a 1:1 complex of ObgE and the 50S ribosomal particle stimulates the ObgE GTPase activity about 120-fold (27). In another study it was shown that the GTPase activity of *Vibrio cholerae* Obg (or CgtA) was also stimulated up to 5-fold by catalytic amounts of 50S or 70S ribosomes (43). Hereto we measured the ObgE_FL activity upon addition of increasing amounts of ribosome. However, at the highest ribosome concentrations we found a significant GTPase activity in the ribosome preparation, most likely due to GTPases that bind and co-purify with the ribosome. After subtracting this background activity we found a gradual increase in the GTPase activity of ObgE with increasing (catalytic) amounts of ribosome (Fig. 7). Addition of 0.1 µM of 70S ribosome to 0.5 µM ObgE increases the initial rate (at 100 µM GTP) about 10-fold. We can thus conclude that while ObgE does not seem to be activated by homodimerization or K$^+$ ions as previously suggested, it is activated upon binding to the ribosome.

Conclusion – ObgE is an essential G protein implicated in ribosome maturation, cell cycle control, DNA replication and bacterial persistence. The present study provides new insights into the structure and function of ObgE. We determined the first crystal structure of ObgE bound to GDP at 1.85 Å resolution and we unequivocally show, using SAXS and MALS, that ObgE behaves as monomer in solution. Biochemical and kinetic analysis unravels a role of the intrinsically disordered C-terminal domain

6

in binding of GTP. Since this domain is less conserved among Obg family members, it remains to be determined whether such a role for this domain is general. Finally, it has been suggested lately that the GTPase activity of Obg proteins might be accelerated by an alternative mechanism, such as homodimerization or binding of K^+ ions. We show that neither of these hypotheses are valid, but rather confirm that the GTPase activity is stimulated in the presence of ribosomes. These findings thus contribute to our understanding of the detailed molecular mechanism of Obg proteins, which in turn might lead to novel insights into the role of ObgE in cellular physiology, including bacterial persistence.

EXPERIMENTAL PROCEDURES

Protein expression and purification - The open reading frame (ORF) coding for full-length ObgE (ObgE_FL) was amplified by PCR from genomic *E. coli* DNA as described before (38), and subsequently cloned within the NdeI and HindIII restriction sites of a pET28 vector containing an N-terminal His_6 tag. In addition, another ObgE_FL construct was cloned with a C-terminal strep tag in a pET22b vector within the NdeI and XhoI restriction sites. An ObgE construct, lacking the last 50 amino acids (ObgE_340), was generated by replacing the codon for Glu341 by a stop codon in pET28-ObgE_FL using the QuickChange site-directed mutagenesis method (Stratagene).

All protein constructs were expressed in either *E. coli* BL21(DE3) or Rosetta (DE3) pLysS cells. Cells were grown in TB medium at 37°C and induced with 1 mM IPTG when an OD_{600} of 0.7 was reached. After induction for 6 h at 25°C, cells were harvested by centrifugation and resuspended in buffer A (20 mM Hepes/NaOH pH 7.5, 300 mM NaCl, 5 mM $MgCl_2$, 5 mM β-mercaptoethanol, 5% glycerol) containing protease inhibitors (AEBSF and leupeptin, 0.1 mg/ml and 1μ/ml final concentrations respectively). After cell disruption using a cell disruptor system (Constant Systems) and clearance of the lysate by centrifugation at 30,000 x g, the supernatant with His_6-tagged proteins was applied to a Ni^{2+}-Sepharose HP column (GE Healthcare), equilibrated with buffer A. After extensive washing with buffer A containing increasing amounts of imidazole (20 mM and 30 mM), the protein was eluted with buffer A containing 250 mM imidazole. In the case of the C-terminal strep-tagged protein, the supernatant

of the cell lysate was loaded on a *Strep-tactin* column (iba life science), washed extensively with buffer A and eluted with buffer A containing 2.5 mM desthiobiotin.

Preparation of nucleotide-free ObgE was achieved by incubation with calf intestine alkaline phosphatase (Roche Diagnostics) followed by dialysis against buffer A. The nucleotide load of the protein was monitored via reversed phase chromatography on a C18 column (Jupiter, 25 cm x 4.6 mm) coupled to an Alliance HPLC (Waters) system as described previously (47). The residual alkaline phosphatase was removed by Ni^{2+}-Sepharose HP (for His_6 tagged ObgE) or a HiTrap Q HP anion exchange (for strep tagged ObgE) column. Size-exclusion chromatography (Superdex75, 16/60) in buffer containing 20 mM Hepes/NaOH pH 7.5, 150 mM NaCl, 5 mM $MgCl_2$ and 2 mM DTT was used as the final purification step. Fractions containing purified ObgE were concentrated, flash frozen in liquid nitrogen and stored at -80°C. All subsequent experiments were started from these nucleotide-free Obg protein batches.

Purification of 70S Ribosome - 15 g (wet weight) of *E. coli* MRE600 cells grown in LB medium were resuspended in a buffer solution containing 20 mM Tris/HCl pH 7.5, 10 mM $MgCl_2$, 100 mM NH_4Cl and 6 mM β-mercaptoethanol (buffer B). Cells were lysed by two passes through a cell disruptor system (Constant Systems). The lysate was centrifuged twice in a Beckman JA-20 rotor at 17000 rpm for 30 min. Subsequently the supernatant was loaded onto two 35 mL sucrose cushions (1.1 M sucrose, 20 mM Tris/HCl pH 7.5, 500 mM NH_4Cl, 10 mM $MgCl_2$ and 0.5 mM EDTA) in 75 mL ultracentrifuge polycarbonate tubes, and centrifuged for 20 h at 35000 rpm at 4°C in a Ti-45 Beckman rotor. The translucent ribosome pellet was gently washed with buffer B. The pellet was resuspended in 5 mL of the same buffer and the volume was adjusted to 100 mL with buffer B containing 0.5 M NH_4Cl. An ultracentrifugation step for 6 h at 25000 rpm was repeated and the pellet was washed with buffer B again. The purified ribosomes were resuspended in 1.6 mL of buffer B containing 50 mM Tris/HCl pH 7.5. The ribosome concentration was calculated using a $\varepsilon_{260\ nm}$ of 4.35 x 10^7 $M^{-1}cm^{-1}$. Finally, the ribosomes were flash frozen in liquid nitrogen and stored at -80°C.

Crystallization, data collection, phasing and refinement - ObgE_340 was loaded with 1 mM GDP and crystals were obtained by mixing

7

protein (at a concentration of 8 mg/mL) with an equal volume of crystallization buffer in a hanging drop vapor diffusion set-up. The crystallization solution contained 16% (w/v) polyethylene glycol (PEG) 6000, 15% (v/v) 2-propanol and 100 mM Sodium Citrate/HCl pH 5.6. Crystals were flash frozen in liquid nitrogen using crystallization buffer supplemented with 15% glycerol as cryoprotectant, and data were collected at 100 K at the PROXIMA II beamline of the Soleil Synchrotron (Paris, France). Data indexing, integration and scaling were done using the XDS suite (48). Data quality was assessed in phenix.xtriage (49). Crystals belong to the space group C222$_1$ with unit cell dimensions a= 64.6 Å, b= 83.0 Å, c= 177.4 Å and α=β=γ= 90° (Table 1).

Phases were obtained by molecular replacement using PHASER (50, 51) from the CCP4 software package (52) and using the structure of *B. subtilis* Obg (PDB: 1LNZ) as search model. ARP/wARP was used for automated model building (53). Model building was finalized by manual building cycles in COOT (54), alternated with refinement in Refmac (55). TLS refinement was implemented in the refinement protocol, using six individual TLS groups determined by the TLSMD server (56, 57). The obtained model was validated with the Molprobity server (58). All figures were prepared in PyMOL (http://www.pymol.org/). Data collection and refinement statistics are summarized in Table1.

SAXS measurement and modeling - Small angle X-ray scattering (SAXS) data for ObgE_FL and ObgE_340 (C-terminal Strep-tag and N-terminally His$_6$ tagged constructs, respectively) were collected either at the SWING beamline of the Soleil Synchrotron (Paris, France) or using an in house Rigaku BioSAXS-2000 instrument. Measurements of ObgE_FL and ObgE_340 in nucleotide-free state and in presence of GppNHp and of ObgE_FL in presence of GDP were performed using an in-line HPLC-SEC setup at the SWING beamline (59). The scattering intensities were recorded after injection of 70 μL of 8-15 mg/ml of protein on an Agilent Bio-SEC 3 column pre-equilibrated with 20 mM Hepes/NaOH pH 7.5, 300 mM NaCl, 250 mM imidazole, 5 mM MgCl$_2$, and 2 mM DTT (SEC buffer) using a flow rate of 0.2 ml/min. For measurements of ObgE_340 in presence of GDP, 1 ml of concentrated protein sample (10 mg/ml) was injected on a S75 10/300 column pre-equilibrated with SEC buffer and connected to an AKTA purifier (GE Healthcare) using a flow rate

of 1.0 ml/min, and subsequently the elution fractions of the protein peak were collected and concentrated to 2.0, 4.0, and 8.0 mg/ml. The SAXS data were immediately afterwards collected in batch mode on a Rigaku BioSAXS-2000 instrument. For data collection of nucleotide-bound proteins, the protein was pre-incubated with 1 mM of the nucleotide, and 400 μM of the corresponding nucleotide was added to the running buffer of the size-exclusion chromatography.

The radial averaging and buffer subtraction of the resulting data frames were performed using FOXTROT for the data collected at the synchrotron and using Rigaku SAXSLab for the data collected on the Rigaku BioSAXS-2000 instrument. A final scattering curve used for processing of the data collected in house, was obtained by merging the lower q value data of the 4.0 mg/ml curve with the higher q value data of the 8.0 mg/ml curve. In case of data collection at the synchrotron, DATASW was used for calculation of the invariants (60). The averaged data, corresponding to a peak of interest, was further processed using ATSAS (61) and SCATTER (42) software packages. The molecular mass of the scattering particle was derived using the Q$_R$ method (42) and Porod-Volume (62). Further interpretation of the SAXS data involved representation using the dimensionless Kratky plot and calculation of the pair-distance distribution function using the ATSAS program GNOM (63), whereas calculation of the theoretical scattering profile of the X-ray crystal structure was done using CRYSOL (64).

Prior to flexibility assessment, two short internal regions within the ObgE_340 structure (residues 133-136 and residues 339-340), missing from the crystal structure, were modeled using the "model missing loop" tool of MODELLER within CHIMERA (65). A similar procedure was performed for ObgE_FL before modelling the flexible C-terminal domain including the C-terminal purification tag. For flexibility assessment of ObgE_340, the crystal structure with modeled loops and the amino acid sequence of the 340 residues of the protein along with the 20 residues of N-terminal purification tag were used. On the other hand, for ObgE_FL, the amino acid sequence of all 390 residues together with the C-terminal purification tag was used. In both cases, a random pool of structures was generated using the EOM suite (66), which gives the combination of an all-atom model, corresponding

8

to the crystal structure, and the C-α traces of the missing flexible regions. Next, a computational pipeline FULCHER (Shkumatov A. *et al*, in preparation) was used to convert the random pool of combined all-atom/C-α trace models to all-atom models, with subsequent model validation using the Molprobity clash score and iterative normal mode analysis (NMA) refinement of the top 50% scoring models to probe the conformational dynamics of the molecule. Finally, the genetic algorithm GAJOE was used to obtain an ensemble of models that best describes the experimental SAXS data. Selected ensembles included refined models that had RMSD <0.4 Å compared to the initial crystal structure.

Multi-angle light scattering (MALS) analysis - Multi-angle light scattering experiments coupled to size exclusion chromatography (SEC-MALS) were performed using a Dawn Heleos (Wyatt technology) detector (using 9 angles) connected to an Agilent Bio-SEC 3 or Shodex KW-800 column attached to an HPLC system (Waters). 10-20 µL of ObgE_FL (with N-terminal His$_6$ tag) at 4-8 mg/ml was injected on the column at a flow rate of 0.2 ml/min in 20 mM Hepes/NaOH pH 7.5, 150 mM NaCl, 5 mM MgCl$_2$ and 2 mM DTT. In case of nucleotide bound sample, the buffer was supplemented with 400 uM of GppNHp or 1 mM of GDP-AlFx. The molar mass was calculated with the ASTRA 5.3.4.20 software.

Steady state kinetic measurements - GTP hydrolysis rates of ObgE were measured by following the production of GDP in function of time on HPLC (Waters). All measurements were performed at 25°C in 20 mM Hepes/NaOH pH 7.5, 150 mM NaCl, 5 mM MgCl$_2$ and 2 mM DTT. For multi-turnover analysis, 0.5 µM of ObgE was incubated with different GTP concentrations ranging from 2.5 until 100 µM. At different time points 50 µl aliquots were taken and the reaction was stopped by heating for 5 min at 100°C. Hydrolysis of GTP was monitored by separation of the nucleotides (GTP and GDP) using a C18 column (Jupiter, 25 cm x 4.6 mm) attached to an HLPC Alliance system (Waters). The nucleotides were eluted using a buffer solution containing 100 mM KH$_2$PO$_4$ pH 6.4, 10 mM tetrabutyl ammonium bromide and 7.5% acetonitrile, as mobile phase. Nucleotides were detected at 254 nm and peak areas were converted to concentration using a standard curve derived from known GDP concentrations. Initial rates were obtained as the slope of the [GDP] versus time plot and fitted to the Michaelis-Menten equation.

The influence of the 70S ribosome on ObgE GTPase activity was determined by pre-incubating increasing amounts of the 70S ribosome (0.01 µM, 0.02 µM, 0.05 µM and 0.1 µM) with 0.5 µM ObgE at 25°C for 30 min. GTPase activity was determined at 100 µM GTP. Since a low GTPase activity co-purified with the ribosome, identical time traces were recorded in absence of ObgE at each ribosome concentration. These time traces were subtracted from the measurements in presence of ObgE before calculating initial rates.

Fluorescence stopped flow kinetics - Nucleotide binding kinetics were determined via fluorescence-stopped flow (SX18.MV; Applied Photophysics). ObgE in a concentration range of 2-16 µM was rapidly mixed with 0.2 µM of 2'/3' N-Methylanthraniloyl-labeled nucleotides (mant-GDP/mant-GTP; Jena Bioscience), providing conditions for pseudo-first order binding kinetics. Mant nucleotides were excited at 360 nm and the change in fluorescence was monitored through a 405 nm cut-off filter. For each protein concentration, the data of at least 5 time traces were averaged and fitted to a single exponential function, yielding the observed rate constant k$_{obs}$. The association and dissociation rate constant (k$_{on}$ and k$_{off}$) were obtained from the slope and intercept of the plot of k$_{obs}$ versus the protein concentration. Alternatively, k$_{off}$ was obtained by mixing 200 µM of unlabeled nucleotide with a mixture of 0.4 µM of protein and 1.5 µM of mant nucleotide. The resulting time traces were fitted on a single exponential, yielding k$_{off}$. The K$_D$ values were calculated from the ratio of k$_{off}$ and k$_{on}$. The experiments were performed at 25°C in 20 mM Hepes/NaOH pH 7.5, 150 mM NaCl, 5 mM MgCl$_2$ and 2 mM DTT.

Isothermal titration calorimetry - Binding affinity of ObgE for guanosine-3',5'-bisdiphosphate (ppGpp; TriLink Biotechnologies) was determined by isothermal titration calorimetry (ITC), using the MicroCal iTC200 system (GE Healthcare, Northampton, MA, USA) with a reference power of 10 microcal/s. The thermodynamic parameters upon titration of ppGpp (750 µM) to nucleotide free ObgE (75 µM) were measured at 25°C in a buffer consisting of 20 mM Hepes/NaOH pH 7.5, 150 mM NaCl, 5 mM MgCl$_2$ and 2 mM DTT. For each experiment a preliminary 0.4 µL injection (not included in data analysis) was followed by 20 injections of each 2 µL with duration of 4 s at a stirring speed of 400 rpm and intervals of 180 s.

The initial delay was 120 s. All experiments were performed in triplicate. Origin version 7.0 software was used for data integration and fitting to a single binding site model using the standard Marquardt non-linear regression method as provided in the Microcal Origin routines. The equilibrium binding dissociation constant (K_D) as well as the binding stoichiometry (n) reported in the main text are given as the mean $\pm$ s.d. of the three independent measurements.

Conflict of interest: The authors declare that they have no conflicts of interest with the contents of this article.

Author contributions: S.G., R.K.S., M.F., N.V., J.M. and W.V. conceived and designed the experiments. S.G. solved the crystal structure. S.G., J.M. and W.V. performed and analyzed kinetic data. R.K.S. and A.V.S. performed and analyzed SAXS measurements. S.G., R.K.S., and W.V. wrote the paper. All authors reviewed the manuscript.

REFERENCES

1. Bourne, H. R., Sanders, D. A., and McCormick, F. (1990) The GTPase superfamily: a conserved switch for diverse cell functions. *Nature*. **348**, 125–132

2. Caldon, C. E., and March, P. E. (2003) Function of the universally conserved bacterial GTpases. *Curr. Opin. Microbiol.* **6**, 135–139

3. Verstraeten, N., Fauvart, M., Versées, W., and Michiels, J. (2011) The Universally Conserved Prokaryotic GTPases. *Microbiol. Mol. Biol. Rev.* **75**, 507–542

4. Vetter, I. R., and Wittinghofer, A. (2001) The Guanine Nucleotide – Binding Switch in Three Dimensions. *Science*. **294**, 1299–1305

5. Wittinghofer, A., and Vetter, I. R. (2011) Structure-function relationships of the G domain, a canonical switch motif. *Annu. Rev. Biochem.* **80**, 943–971

6. Bos, J., Rehmann, H., and Wittinghofer, A. (2007) GEFs and GAPs : Critical Elements in the Control of Small G Proteins. *Cell*. **129**, 865–877

7. Maracci, C., and Rodnina V., M. (2016) Translational GTPases. *Biopolymers*. **105**, 463–475

8. Mishra K., A., and David, L. G. (2016) Small GTPases and their GAPs. *Biopolymers*. **105**, 431–448

9. Ghosh, A., Praefcke, G. J. K., Renault, L., Wittinghofer, A., and Herrmann, C. (2006) How guanylate-binding proteins achieve assembly-stimulated processive cleavage of GTP to GMP. *Nature*. **440**, 101–104

10. Meyer, S., Wittinghofer, A., and Versées, W. (2009) G-Domain Dimerization Orchestrates the tRNA Wobble Modification Reaction in the MnmE/GidA Complex. *J. Mol. Biol.* **392**, 910–922

11. Byrnes, L. J., and Sondermann, H. (2011) Structural basis for the nucleotide-dependent dimerization of the large G protein atlastin-1/SPG3A. *Proc. Natl. Acad. Sci. U. S. A.* **108**, 2216–2221

12. Gasper, R., Meyer, S., Gotthardt, K., Sirajuddin, M., and Wittinghofer, A. (2009) It takes two to tango: regulation of G proteins by dimerization. *Nat. Rev. Mol. Cell Biol.* **10**, 423–429

13. Scrima, A., and Wittinghofer, A. (2006) Dimerisation-dependent GTPase reaction of MnmE: how potassium acts as GTPase-activating element. *EMBO J.* **25**, 2940–2951

14. Anand, B., Surana, P., and Prakash, B. (2010) Deciphering the catalytic machinery in 30S ribosome assembly GTPase YqeH. *PLoS One*. **5**, e9944

15. Ash, M.-R., Maher, M. J., Mitchell Guss, J., and Jormakka, M. (2012) The cation-dependent G-proteins: In a class of their own. *FEBS Lett.* **586**, 2218–2224

16. Rafay, A., Majumdar, S., and Prakash, B. (2012) Exploring potassium-dependent GTP hydrolysis in TEES family GTPases. *FEBS Open Bio.* **2**, 173–177

17. Fislage, M., Wauters, L., and Versées, W. (2016) MnmE , a GTPase that drives a complex tRNA modification reaction. *Biopolymers*. **105**, 568–579

18. Leipe, D. D., Wolf, Y. I., Koonin, E. V, and Aravind, L. (2002) Classification and evolution of P-loop GTPases and related ATPases. *J. Mol. Biol.* **317**, 41–72

19. Buglino, J., Shen, V., Hakimian, P., and Lima, C. D. (2002) Structural and biochemical analysis of the Obg GTP binding protein. *Structure*. **10**, 1581–1592

20. Kukimoto-Niino, M., Murayama, K., Inoue, M., Terada, T., Tame, J. R. H., Kuramitsu, S.,

Shirouzu, M., and Yokoyama, S. (2004) Crystal structure of the GTP-binding protein Obg from Thermus thermophilus HB8. *J. Mol. Biol.* **337**, 761–770

21. Hirano, Y., Ohniwa, R. L., Wada, C., Yoshimura, S. H., and Takeyasu, K. (2006) Human small G proteins, ObgH1, and ObgH2, participate in the maintenance of mitochondria and nucleolar architectures. *Genes to Cells*. **11**, 1295–1304

22. Bang, W. Y., Hata, A., Jeong, I. S., Umeda, T., Masuda, T., Chen, J., Yoko, I., Suwastika, I. N., Kim, D. W., Im, C. H., Lee, B. H., Lee, Y., Lee, K. W., Shiina, T., and Bahk, J. D. (2009) AtObgC, a plant ortholog of bacterial Obg, is a chloroplast-targeting GTPase essential for early embryogenesis. *Plant Mol. Biol.* **71**, 379–390

23. Kotani, T., Akabane, S., Takeyasu, K., Ueda, T., and Takeuchi, N. (2013) Human G-proteins, ObgH1 and Mtg1, associate with the large mitochondrial ribosome subunit and are involved in translation and assembly of respiratory complexes. *Nucleic Acids Res.* **41**, 3713–3722

24. Koller-Eichhorn, R., Marquardt, T., Gail, R., Wittinghofer, A., Kostrewa, D., Kutay, U., and Kambach, C. (2007) Human OLA1 defines an ATPase subfamily in the Obg family of GTP-binding proteins. *J. Biol. Chem.* **282**, 19928–19937

25. Cheung, M.-Y., Li, X., Miao, R., Fong, Y.-H., Li, K.-P., Yung, Y.-L., Yu, M.-H., Wong, K.-B., Chen, Z., and Lam, H.-M. (2016) ATP binding by the P-loop NTPase OsYchF1 (an unconventional G protein) contributes to biotic but not abiotic stress responses. *Proc. Natl. Acad. Sci. U. S. A.* **113**, 2648–2653

26. Kint, C., Verstraeten, N., Hofkens, J., Fauvart, M., and Michiels, J. (2014) Bacterial Obg proteins: GTPases at the nexus of protein and DNA synthesis. *Crit. Rev. Microbiol.* **40**, 207–224

27. Feng, B., Mandava, C. S., Guo, Q., Wang, J., Cao, W., Li, N., Zhang, Y., Zhang, Y., Wang, Z., Wu, J., Sanyal, S., Lei, J., and Gao, N. (2014) Structural and functional insights into the mode of action of a universally conserved Obg GTPase. *PLoS Biol.* **12**, e1001866

28. Trach, K., and Hoch, J. A. (1989) The Bacillus subtilis spo0B Stage 0 sporulation operon encodes an essential GTP-binding protein. *J. Bacteriol.* **171**, 1362–1371

29. Kok, J., Trach, K. A., and Hoch, J. A. (1994) Effects on Bacillus subtilis of a conditional lethal mutation in the essential GTP-binding protein Obg. *J. Bacteriol.* **176**, 7155–7160

30. Okamoto, S., and Ochi, K. (1998) An essential GTP-binding protein functions as a regulator for differentiation in Streptomyces coelicolor. *Mol. Microbiol.* **30**, 107–119

31. Datta, K., Skidmore, J. M., Pu, K., and Maddock, J. R. (2004) The Caulobacter crescentus GTPase CgtAC is required for progression through the cell cycle and for maintaining 50S ribosomal subunit levels. *Mol. Microbiol.* **54**, 1379–1392

32. Foti, J. J., Schienda, J., Sutera, V. a, and Lovett, S. T. (2005) A bacterial G protein-mediated response to replication arrest. *Mol. Cell.* **17**, 549–560

33. Raskin, D. M., Judson, N., and Mekalanos, J. J. (2007) Regulation of the stringent response is the essential function of the conserved bacterial G protein CgtA in Vibrio cholerae. *Proc. Natl. Acad. Sci. U. S. A.* **104**, 4636–4641

34. Kint, C. I., Verstraeten, N., Wens, I., Liebens, V. R., Hofkens, J., Versées, W., Fauvart, M., and Michiels, J. (2012) The Escherichia coli GTPase ObgE modulates hydroxyl radical levels in response to DNA replication fork arrest. *FEBS J.* **279**, 3692–3704

35. Wout, P., Pu, K., Sullivan, S. M., Reese, V., Zhou, S., Lin, B., and Maddock, J. R. (2004) The Escherichia coli GTPase CgtA Cofractionates with the 50S Ribosomal Subunit and Interacts with SpoT, a ppGpp Synthase/Hydrolase. *J. Bacteriol.* **186**, 5249–5257

36. Jiang, M., Sullivan, S. M., Wout, P. K., and Maddock, J. R. (2007) G-Protein Control of the Ribosome-Associated Stress Response Protein SpoT. *J. Bacteriol.* **189**, 6140–6147

37. Persky, N. S., Ferullo, D. J., Cooper, D. L., Moore, H. R., and Susan, T. (2010) The Obg/CgtA GTPase influences the stringent response to amino acid starvation in Escherichia coli. *Mol Microbiol.* **73**, 253–266

38. Verstraeten, N., Knapen, W. J., Kint, C. I., Liebens, V., Van den Bergh, B., Dewachter, L., Michiels, J. E., Fu, Q., David, C. C., Fierro, A. C., Marchal, K., Beirlant, J., Versées, W., Hofkens, J., Jansen, M., Fauvart, M., and Michiels, J. (2015) Obg and Membrane Depolarization Are Part of a Microbial Bet-Hedging Strategy that Leads to Antibiotic Tolerance. *Mol. Cell.* **59**, 9–21

39. Dosztanyi, Z., Csizmok, V., Tompa, P., and Simon, I. (2005) IUPred: Web server for the prediction of intrinsically unstructured regions of proteins based on estimated energy content. *Bioinformatics.* **21**, 3433–3434

40. Dosztanyi, Z., Csizmok, V., Tompa, P., and Simon, I. (2005) The pairwise energy content estimated from amino acid composition discriminates between folded and intrinsically unstructured proteins. *J. Mol. Biol.* **347**, 827–839

41. Scheffzek, K., Ahmadian, M. R., Kabsch, W., Wiesmüller, L., Lautwein, A., Schmitz, F., and Wittinghofer, A. (1997) The Ras-RasGAP Complex: Structural Basis for GTPase Activation and Its Loss in Oncogenic Ras Mutants. *Science* **277**, 333–338

42. Rambo, R. P., and Tainer, J. A. (2013) Accurate assessment of mass, models and resolution by small-angle scattering. *Nature.* **496**, 477–481

43. Chatterjee, A., and Datta, P. P. (2015) Two conserved amino acids of juxtaposed domains of a ribosomal maturation protein CgtA sustain its optimal GTPase activity. *Biochem. Biophys. Res. Commun.* **461**, 636–641

44. Ash, M. R., Guilfoyle, A., Clarke, R. J., Guss, J. M., Maher, M. J., and Jormakka, M. (2010) Potassium-activated GTPase reaction in the G protein-coupled ferrous iron transporter B. *J. Biol. Chem.* **285**, 14594–14602

45. Achila, D., Gulati, M., Jain, N., and Britton, R. A. (2012) Biochemical characterization of ribosome assembly GTPase RbgA in Bacillus subtilis. *J. Biol. Chem.* **287**, 8417–8423

46. Foucher, A. E., Reiser, J. B., Ebel, C., Housset, D., and Jault, J. M. (2012) Potassium Acts as a GTPase-Activating Element on Each Nucleotide-Binding Domain of the Essential Bacillus subtilis EngA. *PLoS One.* **7**, e46795

47. Fislage, M., Brosens, E., Deyaert, E., Spilotros, A., Pardon, E., Loris, R., Steyaert, J., Garcia-Pino, A., and Versées, W. (2014) SAXS analysis of the tRNA-modifying enzyme complex MnmE/MnmG reveals a novel interaction mode and GTP-induced oligomerization. *Nucleic Acids Res.* **42**, 5978–5992

48. Kabsch, W. (2010) *XDS. Acta Crystallogr. Sect. D Biol. Crystallogr.* **66**, 125–132

49. Adams, P. D., Afonine, P. V., Bunkóczi, G., Chen, V. B., Davis, I. W., Echols, N., Headd, J. J., Hung, L. W., Kapral, G. J., Grosse-Kunstleve, R. W., McCoy, A. J., Moriarty, N. W., Oeffner, R., Read, R. J., Richardson, D. C., Richardson, J. S., Terwilliger, T. C., and Zwart, P. H. (2010) PHENIX: A comprehensive Python-based system for macromolecular structure solution. *Acta Crystallogr. Sect. D Biol. Crystallogr.* **66**, 213–221

50. McCoy, A. J. (2006) Solving structures of protein complexes by molecular replacement with Phaser. *Acta Crystallogr. Sect. D Biol. Crystallogr.* **63**, 32–41

51. McCoy, A. J., Grosse-Kunstleve, R. W., Adams, P. D., Winn, M. D., Storoni, L. C., and Read, R. J. (2007) Phaser crystallographic software. *J. Appl. Crystallogr.* **40**, 658–674

52. Winn, M. D., Ballard, C. C., Cowtan, K. D., Dodson, E. J., Emsley, P., Evans, P. R., Keegan, R. M., Krissinel, E. B., Leslie, A. G. W., McCoy, A., McNicholas, S. J., Murshudov, G. N., Pannu, N. S., Potterton, E. A., Powell, H. R., Read, R. J., Vagin, A., and Wilson, K. S. (2011) Overview

of the CCP4 suite and current developments. *Acta Crystallogr. Sect. D Biol. Crystallogr.* **67**, 235–242

53. Langer, G., Cohen, S. X., Lamzin, V. S., and Perrakis, A. (2008) Automated macromolecular model building for X-ray crystallography using ARP/wARP version 7. *Nat. Protoc.* **3**, 1171–1179

54. Emsley, P., and Cowtan, K. (2004) Coot: Model-building tools for molecular graphics. *Acta Crystallogr. Sect. D Biol. Crystallogr.* **60**, 2126–2132

55. Murshudov, G. N., Vagin, A. A., and Dodson, E. J. (1997) Refinement of macromolecular structures by the maximum-likelihood method. *Acta Crystallogr. Sect. D Biol. Crystallogr.* **53**, 240–255

56. Painter, J., and Merritt, E. A. (2006) Optimal description of a protein structure in terms of multiple groups undergoing TLS motion. *Acta Crystallogr. Sect. D Biol. Crystallogr.* **62**, 439–450

57. Painter, J., and Merritt, E. A. (2006) TLSMD web server for the generation of multi-group TLS models. *J. Appl. Crystallogr.* **39**, 109–111

58. Davis, I. W., Leaver-fay, A., Chen, V. B., Block, J. N., Kapral, G. J., Wang, X., Murray, L. W., Iii, W. B. A., Snoeyink, J., Richardson, J. S., and Richardson, D. C. (2007) MolProbity : all-atom contacts and structure validation for proteins and nucleic acids. *Nucleic Acids Res.* **35**, 375–383

59. David, G., and Perez, J. (2009) Combined sampler robot and high-performance liquid chromatography : a fully automated system for biological small-angle X-ray scattering experiments at the Synchrotron SOLEIL SWING beamline. *J. Appl. Crystallogr.* **42**, 892–900

60. Shkumatov, A. V., and Strelkov, S. V. (2015) DATASW, a tool for HPLC-SAXS data analysis. *Acta Crystallogr. Sect. D Biol. Crystallogr.* **71**, 1347–1350

61. Petoukhov, M. V., Franke, D., Shkumatov, A. V., Tria, G., Kikhney, A. G., Gajda, M., Gorba, C., Mertens, H. D. T., Konarev, P. V., and Svergun, D. I. (2012) New developments in the ATSAS program package for small-angle scattering data analysis. *J. Appl. Crystallogr.* **45**, 342–350

62. Rambo, R. P., and Tainer, J. A. (2011) Characterizing flexible and intrinsically unstructured biological macromolecules by SAS using the Porod-Debye law. *Biopolymers*. **95**, 559–571

63. Svergun, D. I. (1992) Determination of the Regularization Parameter in Indirect- Transform Methods Using Perceptual Criteria. *J. Appl. Crystallogr.* **25**, 495–503

64. Barberato, C., Koch, M. H. J., and Svergun, D. I. (1995) CRYSOL - a Program to Evaluate X-ray Solution Scattering of Biological Macromolecules from Atomic Coordinates. *J. Appl. Crystallogr.* **28**, 768–773

65. Martí-Renom, M. A., Stuart, A. C., Fiser, A., Sánchez, R., Melo, F., and Šali, A. (2000) Comparative Protein Structure Modeling of Genes and Genomes. *Annu. Rev. Biophys. Biomol. Struct.* **29**, 291–325

66. Tria, G., Mertens, H. D. T., Kachala, M., and Svergun, D. I. (2015) Advanced ensemble modelling of flexible macromolecules using X-ray solution scattering. *IUCrJ*. **2**, 207–217

67. Karplus, P. A., and Diederichs, K. (2012) Linking Crystallographic Model and Data Quality. *Science* **336**, 1030–1034

68. Shkumatov, A. V., Chinnathambi, S., Mandelkow, E., and Svergun, D. I. (2011) Structural memory of natively unfolded tau protein detected by small-angle X-ray scattering. *Proteins: Struct., Funct., Bioinf.* **79**, 2122–2131

FOOTNOTES

The atomic coordinates and structure factors for the ObgE_340-GDP structure (code 5M04) have been deposited in the Protein Data Bank (http://wwpdb.org/).

The abbreviations used are: TRAFAC, Translation Factor; SAXS, Small Angle X-ray Scattering; MALS, Multi Angle Light Scatter, GNBPs, Guanine nucleotide binding proteins; GEFs, Guanine nucleotide Exchange Factors; GAPs, GTPase Activating Proteins; GAD, G proteins activated by nucleotide dependent dimerization; hOLA1, human Obg-like ATPase 1; pppGpp, Guanosine-pentaphosphate; ppGpp, Guanosine-tetraphosphate; ORF, Open Reading Frame; AEBSF, 4-(2-Aminoethyl) benzenesulfonyl Fluoride hydrochloride; TLS, Translation/Libration/Screw; EOM, Ensemble Optimization Method; NMA, Normal Mode Analysis; RMSD, Root-Mean-Square Deviation; SEC, Size Exclusion Chromatography; HPLC, High-Performance Liquid Chromatography; ITC, Isothermal Titration Calorimetry.

15

TABLES

TABLE 1. Data collection and refinement statistics

Data collection and processing	ObgE_340 - GDP
X-ray source	SOLEIL PROXIMA II
Wavelength (Å)	1.07812
Resolution range (Å)[a]	49.00-1.85 (1.90-1.85)
Total/Unique reflections	280027/41090 (20519/1943)
R_{meas} (%)	9.7 (182.3)
I/sigI	9.67 (1.00)
$CC_{1/2}$	99.8 (48.9)
Completeness (%)	99.9 (100)
Redundancy	6.81 (6.97)
Spacegroup	$C222_1$
Cell dimensions	
a, b, c (Å)	64.6, 83.0, 177.4
a, b, g (°)	90, 90, 90
Model refinement	
R_{work}/R_{free} (%)[b]	19.8/23.9
RMSD bond length (Å)	0.0154
RMSD bond angle (°)	1.7629
Ramachandran	
favored/allowed/disallowed regions (%)	98.5/0.9/0.6
PDB code	5M04

[a]Values for the highest-resolution shell are given in between brackets. $CC_{1/2}$ values were used as a guide for selecting the highest usable resolution shell (67). [b]A subset of 5% of the reflections was used for calculating R_{free}.

TABLE 2. Steady state kinetic parameters of GTP hydrolysis by wild-type ObgE_FL, ObgE_340 and mutant ObgE_FL. Assays were performed in buffer containing 150 mM NaCl or KCl.

protein	Salt	k_{cat} (min^{-1})	K_M (μM)
ObgE_FL	NaCl	0.064 ± 0.001	10.40 ± 0.70
ObgE_FL	KCl	0.045 ± 0.001	5.64 ± 0.56
ObgE_FL_K183A	NaCl	0.020 ± 0.000	10.27 ± 0.75
ObgE_FL_R177A	NaCl	0.060 ± 0.002	6.63 ± 0.69
ObgE_340	NaCl	0.046 ± 0.001	11.07 ± 0.92

FIGURE LEGENDS

FIGURE 1. The crystal structure of *E. coli* ObgE_340 bound to GDP. (a) Domain organization of ObgE, showing the Obg domain (green), G domain (grey) and C-terminal domain (orange) and the conserved sequence motifs in the G domain (G1-G5, Switch I and II). The structure of a construct lacking the C-terminal domain (ObgE_340) was solved. (b) Cartoon representation of the ObgE_340-GDP crystal structure. The Obg domain and G domain are shown in green and grey respectively with sequence motifs colored in the same way as in (a). GDP is shown as sticks with carbon bonds colored yellow. Mg^{2+} is shown as a green sphere. (c) Close-up view of the GDP binding site of ObgE_340. GDP and Mg^{2+} are colored as in (b). Hydrogen bonds between the protein and the nucleotide are indicated by yellow dotted lines. (d) GDP bound to ObgE_340 with the clearly defined "omit" electron density map, contoured at 2σ, shown as a blue mesh.

FIGURE 2. Potential dimer interface of ObgE_340 generated though crystal symmetry operations. (a) Potential dimer organization of ObgE_340 via a face-to-face interaction of its G domain with the G domain of a neighboring protein molecule in the crystal lattice. The two symmetry variants are colored grey and green, and are labeled ObgE_340 and ObgE_340', respectively. The C-atoms of the bound GDP molecules are colored according to the protomer to which they belong. (b) Close up view of the interaction surface shown in (a). K183 and R177, located on the switch I and the first α-helix of the G domain of one protomer, interact with the phosphate groups of GDP from the adjacent promoter. (c) Superposition of the structure of the Ras-RasGAP complex (in presence of GDP-AlF₃, PDB: 1WQ1 [62]) with the ObgE_340-GDP structure. The two symmetry related protomers of ObgE_340 and GDP are colored and labeled according to (b). Ras and the bound GDP-AlF₃ are colored yellow. The "arginine finger" of RasGAP (R789) is shown in cyan. This superposition shows a spatially similar position of the amino group of K183 in the ObgE_340 – ObgE_340' homodimer and the guanido group of R789 of RasGAP in the Ras-RasGAP complex.

FIGURE 3. SAXS analysis of ObgE_FL and ObgE_340 in their nucleotide-free state, providing information regarding the radius of gyration (R_g), maximum particle dimension (D_{max}) and molecular mass. (a) Averaged scattering profile of ObgE_340 (red) and ObgE_FL (blue). The inset figure shows the linear Guinier region for both constructs, indicative of a non-aggregated protein sample. The deduced R_g values are given. (b) Normalized P(R) profile of ObgE_340 (red) and ObgE_FL (blue). The broader distribution of intramolecular distances and larger value of D_{max} of ObgE_FL reflect the disordered nature of its C-terminal domain. (c) Dimensionless Kratky plot for ObgE_340 (red) and ObgE_FL (blue) in comparison with an intrinsically disordered protein (hTau40wt, cyan trace) and a globular protein (BSA, orange trace) (68). While the shapes of both curves are typical for an elongated protein such as ObgE, comparison of the curves indicates a higher degree of flexibility in ObgE_FL. Raw data underlying the averaged scattering profiles are shown in Fig. S3 and S4.

FIGURE 4. SAXS-based ensemble modelling of ObgE_FL taking into account the flexibility of the C-terminal domain. (a) Ensemble fit of ObgE_FL (red line) to the experimental ObgE_FL SAXS profile (black trace). The residuals are shown at the bottom of the fit (dark green). (b) The R_g distribution of the ensemble (red curve) compared to the R_g distribution of a random pool of models (grey filled area) generated using EOM coupled to all-atom modeling, model validation and NMA-refinement. (c) Ribbon representation of 5 ensemble models, selected by the genetic algorithm, which give an average theoretical curve that fits the experimental ObgE_FL SAXS profile as shown in (a).

FIGURE 5. GDP and GTP binding and dissociation kinetics of ObgE_FL (a, c, e) and ObgE_340 (b, d, f) determined via stopped-flow fluorescence analysis. (a, b) Transients obtained by following mGDP (0.2 / 0.1 µM, before / after mixing) fluorescence upon rapid mixing with different concentrations of ObgE_FL (a) and ObgE_340 (b). Concentration values given on the graph represent ObgE concentrations before and after mixing. The lower panels show the concentration dependency of the observed rate constant (k_{obs}). The slope of the linear fit yields k_{on}. (c, d) Transients obtained by following mGTP (0.2 / 0.1 µM, before / after mixing) fluorescence upon rapid mixing with different concentrations of ObgE_FL (c) and ObgE_340 (d). The same concentrations as in (a) and (b) are used. The lower panels

17

show the concentration dependency of the observed rate constant (k_{obs}). The slope and intercept of the linear fit yield k_{on} and k_{off} respectively. (e, f) Direct determination of k_{off} by following the release of mGDP from ObgE_FL (e) and ObgE_340 (f) upon mixing 200 µM of unlabeled GDP with a mixture of 0.4 µM ObgE and 1.5 µM mGDP. (g) Summary of nucleotide binding/dissociation kinetics and the deduced K_D values of ObgE_FL and ObgE_340.

FIGURE 6. Isothermal titration calorimetry (ITC) experiments for binding of ppGpp to ObgE_FL (a) and ObgE_340 (b) respectively. Experiments were performed at 25°C by titrating ppGpp from a stock solution of 750 µM into a solution of 75 µM nucleotide-free ObgE. Equilibrium dissociation constants (K_D) and binding stoichiometries (n) are given as the mean ± s.d. of 3 independent measurements (all isotherms are given in Supplementary Fig. S9).

FIGURE 7. Stimulation of ObgE GTPase activity by the 70S ribosome. Initial rate kinetic traces (a) and deduced initial rates (b) for GTP (100 µM) hydrolysis by ObgE_FL (0.5 µM) without and with increasing concentrations of 70S ribosome. Time traces and initial rates are shown after subtraction of a background GTPase activity in the ribosomal preparation, probably due to a contaminating GTPase that copurified with the ribosome. Each data point represents the average ± s.d. of 3 independent measurements.

FIGURE 1.
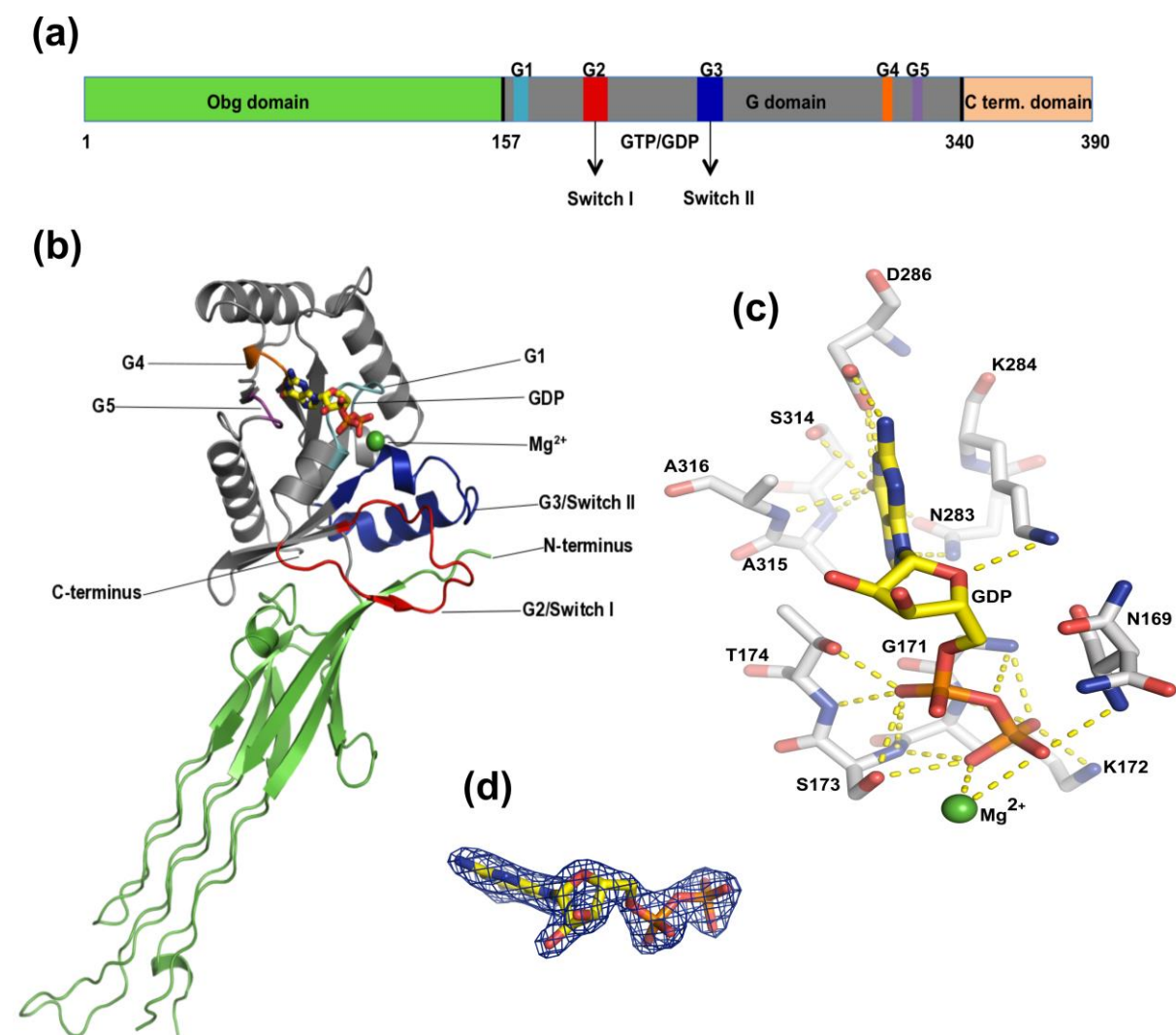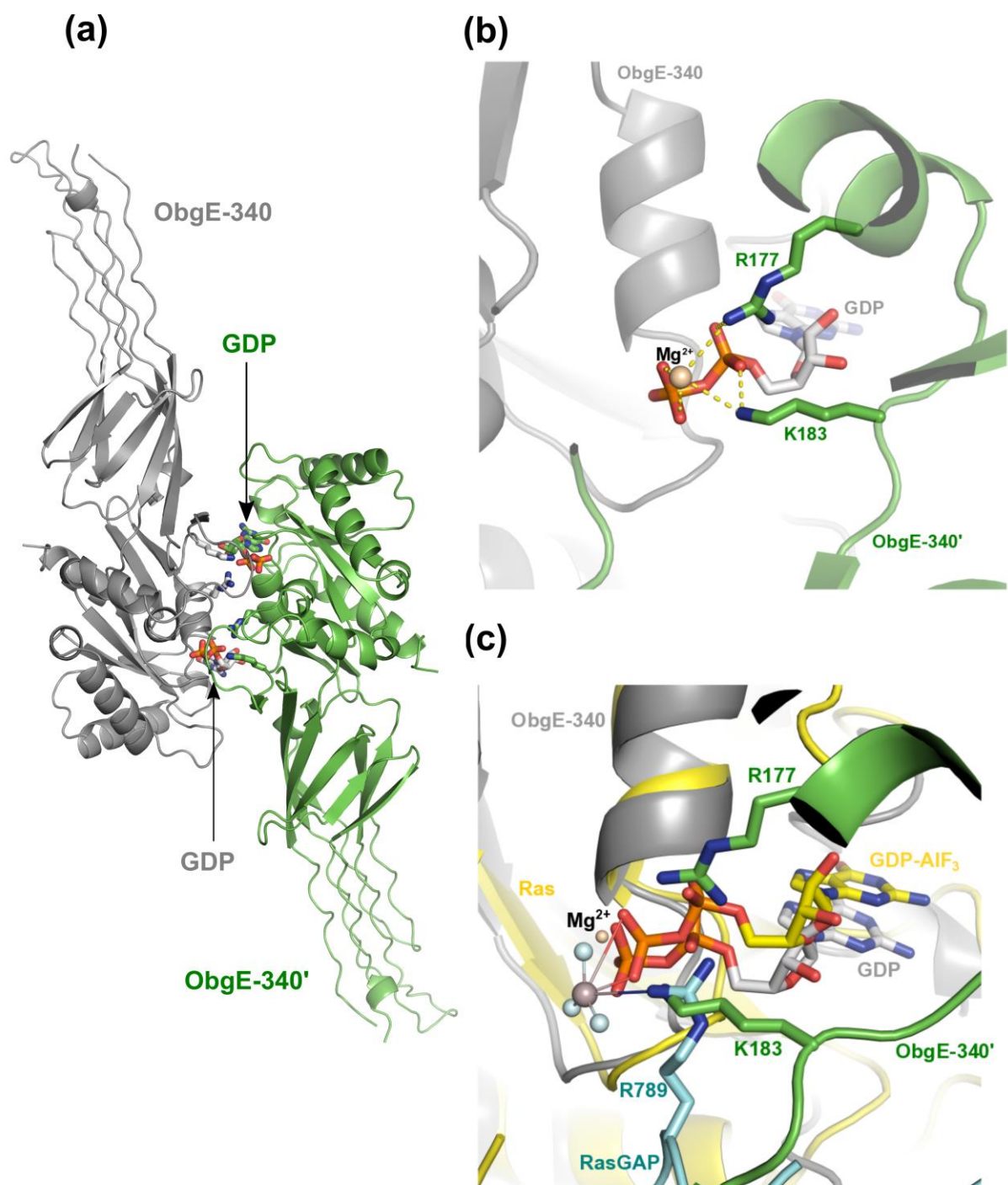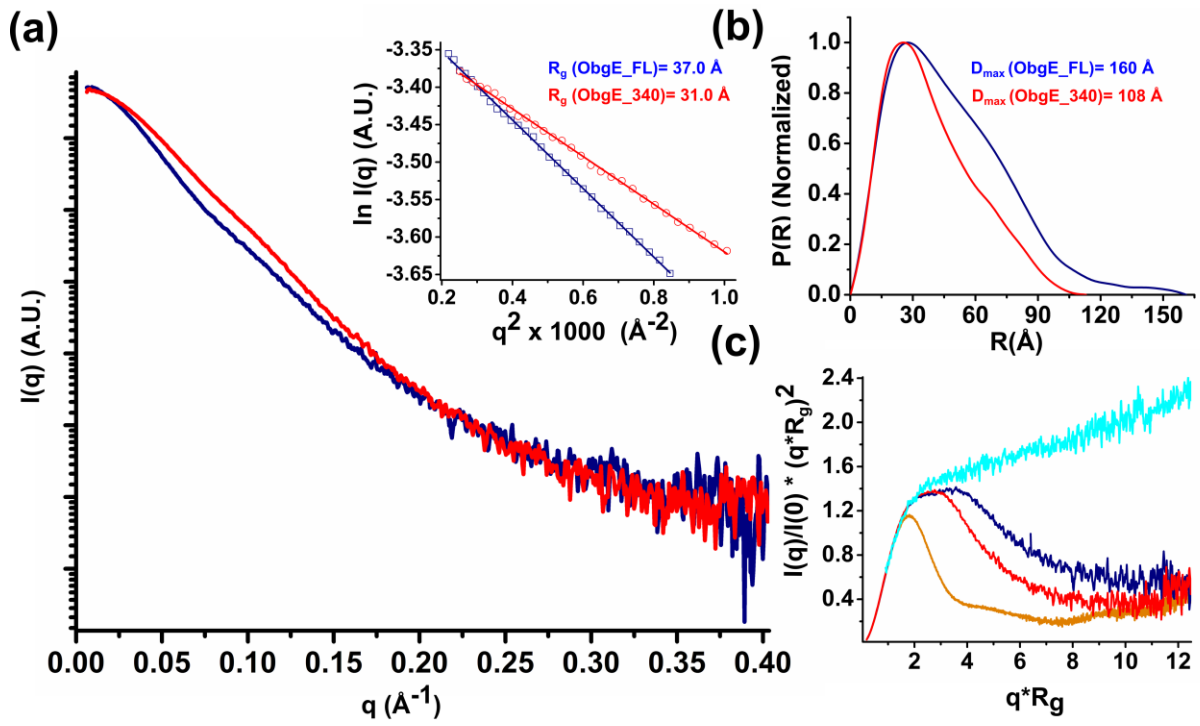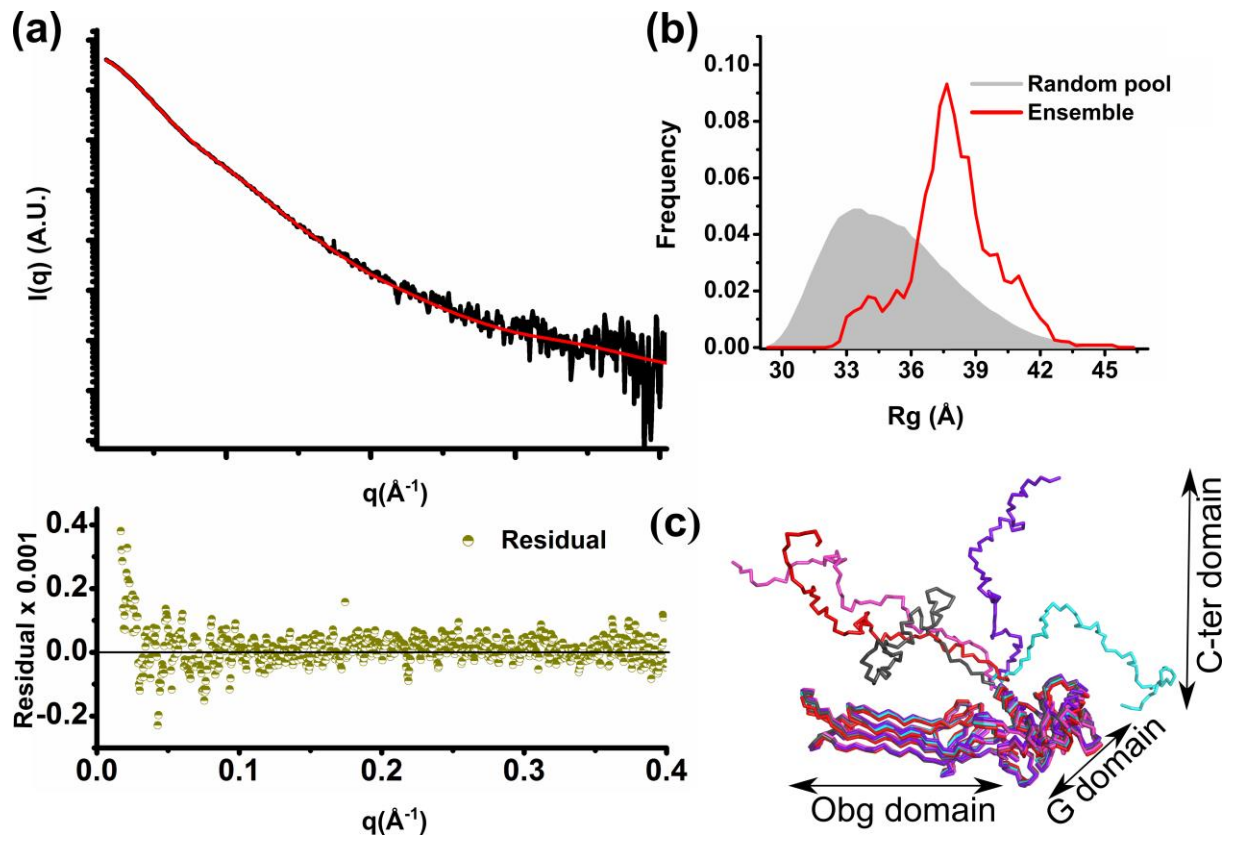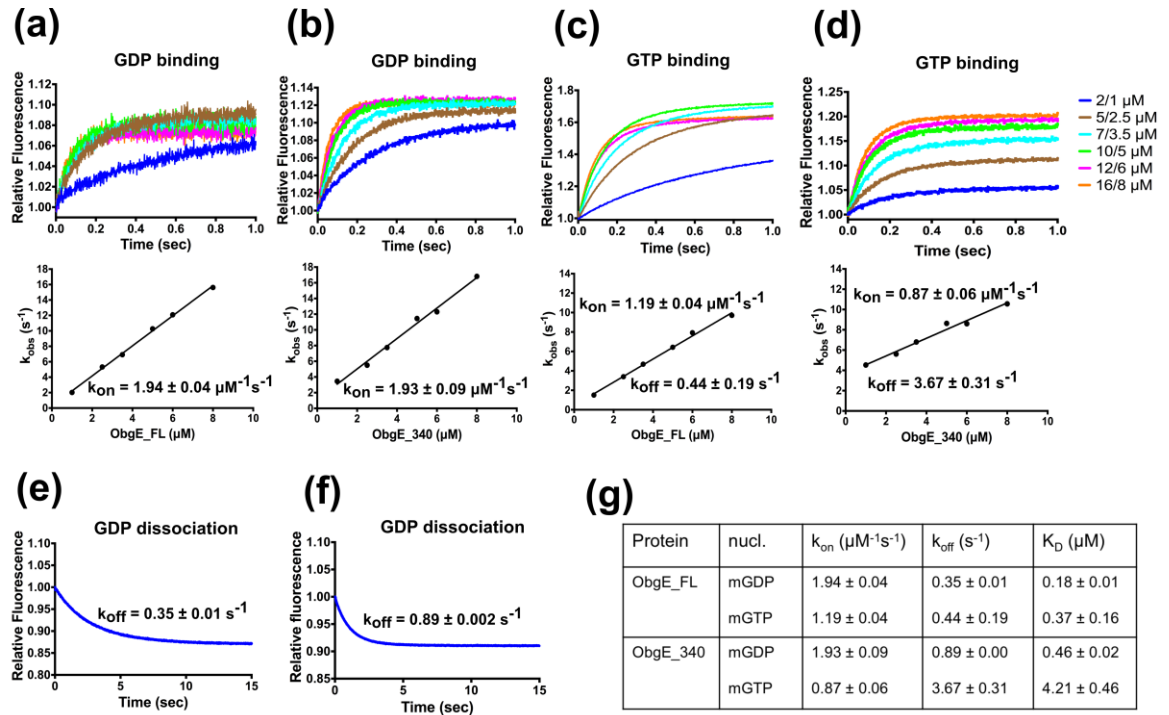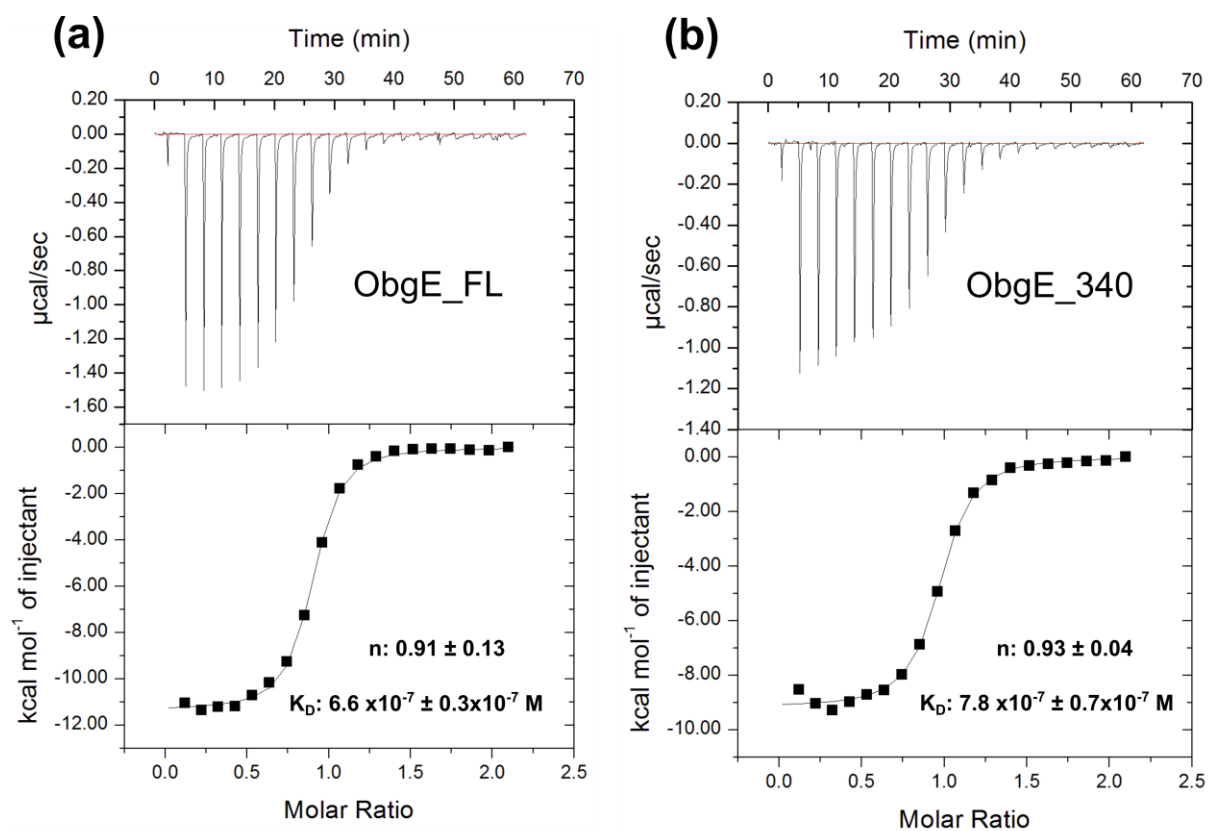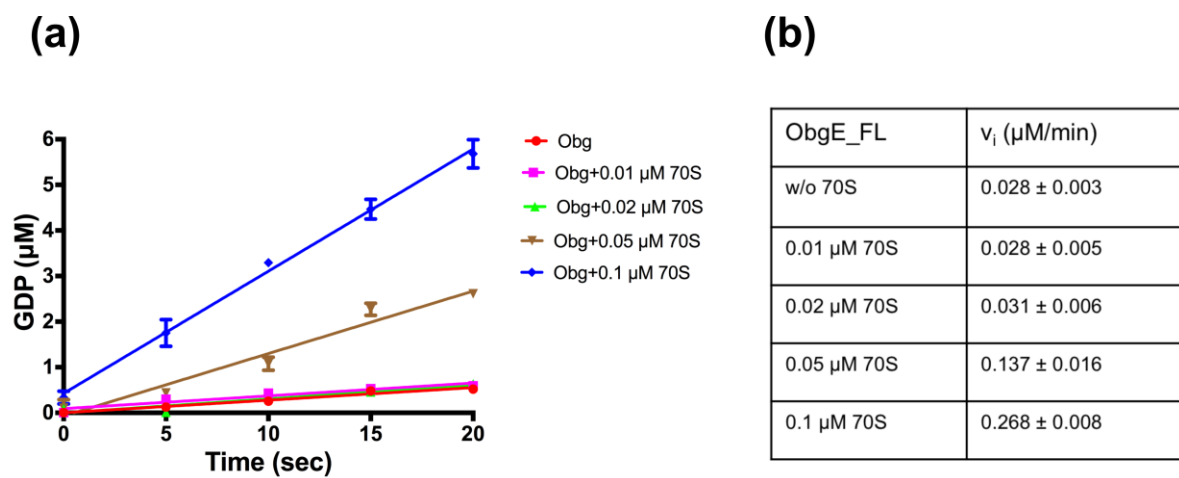
(a)

(b)

(c)

(d)

FIGURE 2.

FIGURE 3.

21

FIGURE 4.

FIGURE 5.

23

FIGURE 6.

(a) ObgE_FL

n: 0.91 ± 0.13

K_D: 6.6 ×10⁻⁷ ± 0.3×10⁻⁷ M

(b) ObgE_340

n: 0.93 ± 0.04

K_D: 7.8 ×10⁻⁷ ± 0.7×10⁻⁷ M

24

FIGURE 7.

(a)

(b)

ObgE_FL	v_i (µM/min)
w/o 70S	0.028 ± 0.003
0.01 µM 70S	0.028 ± 0.005
0.02 µM 70S	0.031 ± 0.006
0.05 µM 70S	0.137 ± 0.016
0.1 µM 70S	0.268 ± 0.008

25

Structural and Biochemical Analysis of *Escherichia coli* ObgE, a Central Regulator of Bacterial Persistence

Sotirios Gkekas, Ranjan Kumar Singh, Alexander V Shkumatov, Joris Messens, Maarten Fauvart, Natalie Verstraeten, Jan Michiels and Wim Versées

Alerts:
- When this article is cited
- When a correction for this article is posted

Click here to choose from all of JBC's e-mail alerts

This article cites 0 references, 0 of which can be accessed free at
http://www.jbc.org/content/early/2017/02/21/jbc.M116.761809.full.html#ref-list-1